Zero-Phase-Angle Controlled Bidirectional Wireless EV Charging Systems for Large Coil Misalignments

Yeran Liu, *Student Member, IEEE*, Udaya Kumara Madawala, *Fellow, IEEE*, Ruikun Mai, *Member, IEEE*, and Zhengyou He, *Senior Member, IEEE*

***Abstract*—Misalignment between charging coils is an unavoidable problem in all electric vehicle (EV) charging systems that are based on wireless power transfer (WPT) technology. This is because variations in both self- and mutual inductances of charging coils due to coil misalignments significantly affect the charging rate and efficiency of the EV charger. As a solution, this article proposes a new control technique that maintains the rated charging power level at optimum efficiency in spite of large coil misalignments. To compensate for the variations in inductances, the technique uses the information extracted from input impedance to operate the system essentially at unique converter voltages with zero phase angle, ensuring that charging will take place at rated power with optimal efficiency despite any pad misalignments. The article presents a comprehensive mathematical model, describing the theoretical basis of the proposed control philosophy. To demonstrate the validity of the proposed control concept, a 1-kW bidirectional WPT EV charging system is built and results are presented under misaligned coil conditions. Results convincingly indicate that the proposed controller is efficient and capable of maintaining the rated charging rate despite large coil misalignments and without any dedicated wireless communication.**

***Index Terms*—Bidirectional, control, misalignment, wireless power transfer (WPT), zero phase angle (ZPA).**

I. Introduction

GLOBALLY electric vehicles (EVs) are now accepted as the means of future transport that addresses energy and emission concerns. EV can be charged using either a wired or wireless power transfer (WPT) technology. Wired charging is the most common way of charging EVs but long charging cables pose trip hazards, and it is not ideal for in harsh and hostile conditions where there are snow, ice, and chemicals. In contrast, wireless EV charging, based on the inductive power transfer technology, is gaining recognition as a convenient way to charge EVs through weak magnetic coupling with no physical connections. WPT enables power transfer across an air-gap and is safe and convenient and, hence, becoming popular in EV charging applications [1]–[8].

EVs can be charged wirelessly when the vehicle is either stationary or moving (dynamic). Irrespective of whether the EV is stationary or moving, one of the main challenges in wireless EV charging is to mitigate the adverse effects caused by the misalignment between charging coils. This is because all wireless charging systems essentially employ resonant networks to minimize the supply of reactive power when charging an EV at the desired power rate. However, in practice the coils cannot be perfectly aligned during charging and, as a consequence, the charging system invariably operates under detuned condition due to variation in magnetic coupling and coil inductances caused by coil misalignment. When detuned, the system draws reactive power, increasing system losses and reducing the charging power level.

A number of techniques, including new control concepts, special coil designs, hybrid coil structures, topologies, etc., have been proposed and implemented to address this problem with varying degrees of success [9]–[26]. Polarized charging pads, such as Double-D (DD) and bipolar pads, have been proposed in [9], [10] to improve the magnetic coupling and the tolerance to pad misalignment. Based on these coil structures, some compensation topologies have also been utilized to further improve power transfer capability. A dual-coupled *LCC* compensation network with compact DD and Q pads has been used in [11] to improve performance under misalignment. Parallel-hybrid and series-hybrid topologies of the *LCL* and *CL* compensation networks have been proposed in [12] and [13] to achieve stable output power and relatively high efficiency. However, without any active control, the design and construction of these passive solutions are complex in nature, in addition to being prone to power fluctuations.

An alternate approach is to adopt active control strategies with common and simple compensation topologies. This approach offers freedom to regulate output power through the control of both primary and secondary converters, and such examples are phase-shift modulation of full-bridge converters [14]–[20] and duty cycle control of dc–dc converters [21]–[24]. Although more control freedom can be achieved with the use of converters, it is also important to establish a criterion that regulates output power while operating the system at its optimal state. In [18], an

Manuscript received April 6, 2019; revised July 28, 2019; accepted September 5, 2019. Date of publication September 15, 2019; date of current version February 11, 2020. This work was supported in part by the National Key R&D Program of China under Grant 2017YFB1201002, in part by China Scholarship Council (CSC) Scholarship under Grant 201807000095, and in part by Sichuan S&T Innovation Project under Grant 2018096. Recommended for publication by Associate Editor O. Lucia. *(Corresponding author: Zhengyou He.)*

Y. Liu and R. Mai are with the Electrical Engineering Department, Southwest Jiaotong University, Chengdu 610031, China (e-mail: yeranliu@my.swjtu.edu.cn; mairk@swjtu.edu.cn).

U. K. Madawala is with the Electrical and Computer Engineering, The University of Auckland, Auckland 92019, New Zealand (e-mail: u.madawala@auckland.ac.nz).

Z. He is with the School of Electrical Engineering, Southwest Jiaotong University, Chengdu 610031, China (e-mail: Hezy@home.swjtu.edu.cn).

Color versions of one or more of the figures in this article are available online at http://ieeexplore.ieee.org.

Digital Object Identifier 10.1109/TPEL.2019.2941709

active rectifier has been used to control the output voltage/current while using a control criterion, independent of the variation in mutual inductance, to calculate the primary converter's optimal pulsewidth, based on the output voltage and the pulsewidth of the active rectifier. In contrast, a mutual inductance estimation method has been proposed in [24] to track the optimal state against the coupling variation via a buck–boost converter on the secondary side, while controlling the output voltage through the primary converter. The Perturb & Observation strategy, proposed in [21] and [22], searches for the optimal operating point without using mutual inductance information, but by calculating system efficiency online and adjusting the duty cycle of converters. The main drawback of these methods is the need for a wireless communication link to exchange information between the primary and secondary sides to achieve the optimal state of operation to minimize losses. In [25], a controller based on the "ON" and "OFF" times of the primary converter has been proposed to eliminate the need for communication, but at the expense of lower efficiency due to loss of resonant energy during the long "OFF" time period. According to literature, a simple and cost-effective technique that restores the rated charging power level at maximum efficiency under large coil misalignments and without any dedicated communication is yet to be reported.

This article therefore proposes a simple control strategy for wireless EV charging systems to maintain the rated charging power level at maximum efficiency even under large coil misalignments and without any direct communication. The technique estimates the phase relationship between the input voltage and current from the input impedance and uses the phase relationship to compensate for the variations in inductances due to coil misalignment. With the proposed technique, the system is operated at zero phase angle (ZPA) and with unique converter voltages to ensure that the output power remains at the rated level and at maximum efficiency despite misalignments in charging coils. A comprehensive mathematical model is presented, describing the theoretical relationship among ZPA, optimal load resistor, coil inductances, and duty cycles of the converters that lead to rated power delivery at maximum efficiency. The proposed method is applicable to both uni- and bidirectional WPT EV charging systems, and its validity is demonstrated through theoretical and simulated results, presented in comparison to measured results of a 1-kW prototype BD-WPT charging system.

II. Circuit Analysis

A. Circuit Modeling

A schematic of a typical series–series (S–S) compensated bidirectional WPT system is shown in Fig. 1(a). The full-bridge converters, used on both sides, are operated either as an inverter or a controlled rectifier at 85 kHz, depending on the direction of power flow. V_o represents the battery voltage of EV, and $V_{\rm dc}$ that feeds the primary-side converter is derived from the grid using a low-frequency converter, which is not shown for brevity. To improve power transfer capability under weak coupling, an S–S resonant network is chosen. L_P and L_S are the self-inductances

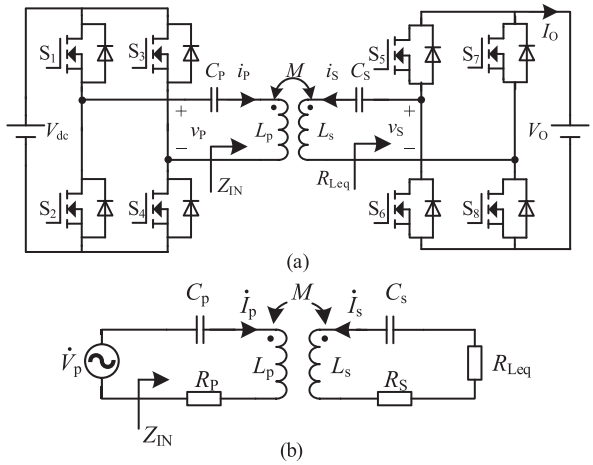

Fig. 1. (a) Bidirectional WPT system with series–series compensation. (b) Fundamental harmonic circuit model during the forward power flow.

of the charging coils, and C_P and C_S are the respective compensation capacitors. *M* is the mutual inductance between the primary and secondary coils.

Fig. 1(b) shows the circuit model at the fundamental frequency, where the voltage produced by the primary converter is represented as a sinusoidal voltage source $\dot{V}_P$ at an angular frequency ω. The secondary converter, which acts a controlled rectifier during the forward power flow, and the dc battery load are represented by an ac equivalent load resistor $R_{\rm Leq}$. The equivalent-series resistors (ESRs) of primary- and secondary-side charging coils are denoted as R_P and R_S, respectively.

Using Kirchhoff's voltage law, the circuit model in Fig. 1(b) can be expressed mathematically by the following equations:

$$\dot{V}_P = Z_P \dot{I}_P + j\omega M \dot{I}_S \tag{1}$$

$$0 = j\omega M \dot{I}_P + Z_S \dot{I}_S + R_{\rm Leq} \dot{I}_S \tag{2}$$

where impedances Z_P and Z_S seen by primary- and secondary-side voltages, respectively, are given by

$$Z_P = j\omega L_P + (j\omega C_P)^{-1} + R_P = jX_P + R_P \tag{3}$$

$$Z_S = j\omega L_S + (j\omega C_S)^{-1} + R_S = jX_S + R_S \tag{4}$$

where X_P and X_S represent the reactance of coil inductances. Both converters are controlled with phase-shift modulation, and the rms voltage $\dot{V}_P$ produced by the primary converter can be expressed as

$$V_P = \frac{2\sqrt{2}}{\pi} \sin\left(\frac{\alpha}{2}\right) V_{\rm dc} \tag{5}$$

where α is the duty cycle of the primary converter, which is related to phase-shift φ_P between the two legs of the converter, through $\alpha = 180^\circ - \varphi_P$.

The relationship between the dc load resistor R_L and the ac equivalent load resistor $R_{\rm Leq}$ can be represented by

$$R_{\rm Leq} = \frac{8}{\pi^2} \sin\left(\frac{\beta}{2}\right)^2 R_L \tag{6}$$

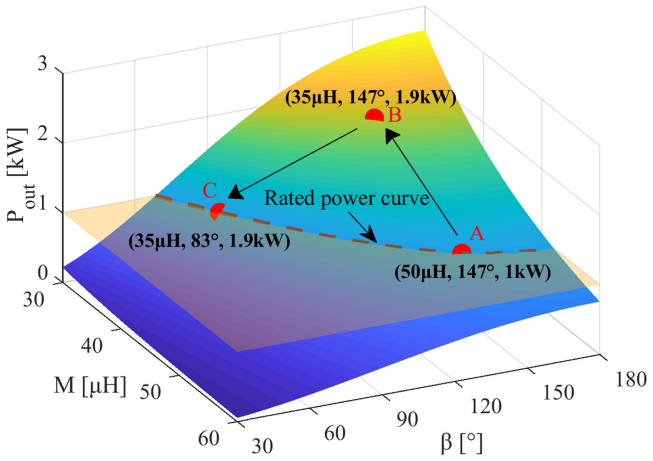

Fig. 2. Output power with various M and β.

where β is the duty cycle of the secondary-side converter, which is related to the phase-shift φ_S between its two legs through $\beta = 180° - \varphi_S$. R_L is an actual load resistor or a dc equivalent load resistor of battery load expressed as

$$R_L = \frac{V_O^2}{P_{\text{out}}} = \frac{V_O}{I_O} \tag{7}$$

where P_{out} and I_O are the charging power and charging current, respectively.

B. Dependence of Output Power on M, α, and β

According to (1), the currents on both sides can be expressed as

$$\dot{I}_P = \dot{V}_P \left(N_{PR} + jN_{PI}\right)/W_P \tag{8}$$

$$\dot{I}_S = \dot{V}_P \left(N_{SR} + jN_{SI}\right)/W_P \tag{9}$$

where

$$\begin{cases} N_{PR} = \omega^2 M^2 \left(R_S + R_{\text{Leq}}\right) + R_P \left[\left(R_S + R_{\text{Leq}}\right)^2 + X_S^2\right] \\ N_{PI} = -X_P(R_S + R_{\text{Leq}})^2 + \omega^2 M^2 X_S - X_P X_S^2 \\ N_{SR} = \omega M(R_P X_S + R_S X_P + X_P R_{\text{Leq}}) \\ N_{SI} = \omega M(X_P X_S - \omega^2 M^2 - R_P R_S - R_P R_{\text{Leq}}) \\ W_P = (X_P^2 + R_P^2)\left[\left(R_S + R_{\text{Leq}}\right)^2 + X_S^2\right] \\ +2\omega^2 M^2(-X_P X_S + R_P R_{\text{Leq}} + R_P R_S + \omega^2 M^2/2). \end{cases}$$

Using the above equations, the input power and output power can be represented by

$$P_{\text{in}} = \text{Re}\left[\dot{V}_P \cdot (\dot{I}_P)^*\right] = V_P^2 N_{PR}/W_P \tag{10}$$

$$P_{\text{out}} = \text{Re}\left[\dot{I}_S \cdot R_{\text{Leq}} \cdot (\dot{I}_S)^*\right] = V_P^2 \omega^2 M^2 R_{\text{Leq}}/W_P \tag{11}$$

where $(\cdot)^*$ is the conjugate of variables. As evident from (11), P_{out} is mainly dependent on V_P, R_{Leq} and M, and hence can be controlled through α and β for any given M, as per (5) and (6). However, there are still an infinite number of combinations of α and β that satisfy (11). Fig. 2 shows the dependence of P_{out} on M and β. The duty cycle α was set to be 120° and V_P was equal to 156 V according to (5). Unless otherwise specified, all the theoretical analysis results and figures are based on the parameters listed in Table I. Note that X_P and X_S are assumed to be constant here because the variations of both L_P and L_S are small in comparison to M, and the sensitivity analysis of X_P and X_S is presented in the next section.

TABLE I
CIRCUIT PARAMETERS FOR THEORETICAL ANALYSIS

Symbol	Parameter	Value	Unit
f	inverter frequency	85	kHz
V_{dc}	input voltage	200	V
V_O	output voltage	200	V
R_L	equivalent dc load resistor for 1kW output power	40	Ω
X_P	reactance in primary side	3	Ω
X_S	reactance in secondary side	3	Ω
R_P	ESR of primary coil	0.3	Ω
R_S	ESR of secondary coil	0.3	Ω
M	mutual inductance	[60.3, 31.6]	μH

For example, consider a situation where the system is operated with α =120° while regulating the output power by controlling β of the secondary converter. In this situation, the rated power is delivered only when M is 50 μH and β is 147°, as illustrated by point A in Fig. 2. Now if M changes from 50 to 35 μH, then the operating point moves to B, increasing output power to 1.9 kW. In order to restore the output power to 1 kW, β must be reduced, forcing the operating point to settle at point C on the rated power curve. In general, if β is controlled to be along the rated power curve in Fig. 2, the system can maintain the rated charging power against the variation of M.

However, P_{out} is also dependent on V_{P}. Thus various $V_P(\alpha)$, will result in various rated power curves. The equivalent load resistor $R_{\text{Leq}O}$ for given P_{out} is a function of $V_P(\alpha)$ and can be solved from (11) as where

$$\begin{cases} Z_M = \omega M \\ K_1 = \omega^2 M^2 R_P + R_S X_P^2 + R_S R_P^2 \\ K_2 = \omega^2 M^2 X_P - X_S X_P^2 - X_S R_P^2. \end{cases}$$

Substituting (5) and (12) shown at the bottom of this page, into (6), the duty cycle of the secondary converter β_O for rated power can be represented by

$$\beta_O = 2\arcsin\left(\sqrt{\frac{8R_{\text{Leq}O}(\alpha)}{\pi^2 R_L}}\right). \tag{13}$$

β_O, as a function of both α and M, is shown in Fig. 3. It is obvious that β_O for constant output power varies with α, which again has many combinations for each M. Moreover, there is also a region where any value of β that is not able to provide rated output power due to small α and relatively large M. This region can be avoided by increasing α or V_{dc}.

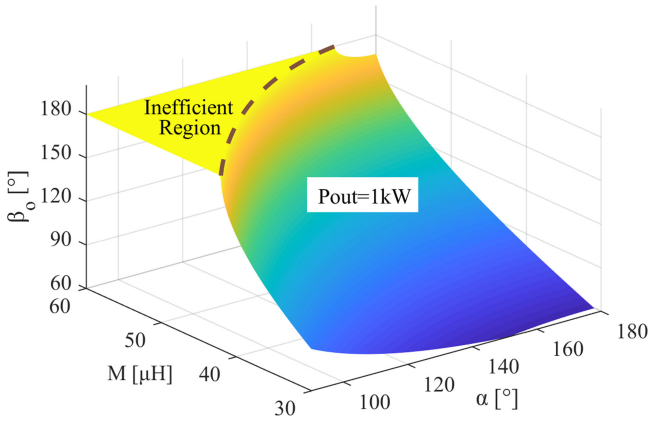

Fig. 3. β_O for constant P_{out} versus M and α.

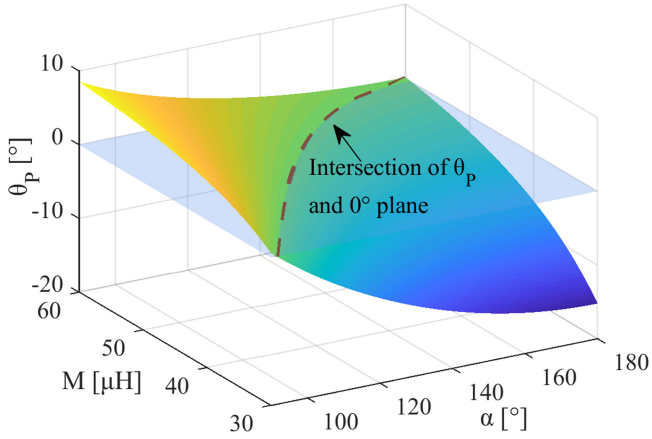

Fig. 4. Variation of θ_P with M and α.

Consequently, determination of the correct α and β combination that gives maximum efficiency, even for this simplified condition, is extremely difficult and involves optimization that cannot be executed real time. However, this difficulty can be overcome as described below.

C. Optimal Combination of α and β for the ZPA Condition

As explained in the previous section and illustrated in Fig. 3, there are endless combinations of α and β for both constant output power and any given M. Moreover, not all combinations of α and β are optimal in relation to system efficiency, and finding the unique combination that corresponds to optimal efficiency is not a simple and straight forward task. However, this challenge can be overcome by using the phase angle θ_P between the input voltage and current, estimated from the input impedance Z_{in} seen by the primary converter, as the criterion for finding the unique and optimal combination of α and β. This is because when the pads are misaligned, the system is detuned (nonresonant) due to variations in self- and mutual inductances and, therefore, θ_P is no longer zero as Z_{in} is now complex. Consequently, the converter inevitably supplies reactive power to the resonant network, increasing overall system losses. However, if the primary converter can be operated with ZPA for any given combination of α and β, the system can be operated at optimal efficiency under any misaligned conditions to deliver rated power, as described below.

The input impedance Z_{IN} is the sum of the self-impedance in the primary side and the reflected impedance from the secondary side and can be expressed as

$$Z_{\text{IN}} = R_P + \frac{\omega^2 M^2 \left(R_S + R_{\text{Leq}}\right)}{\left(R_S + R_{\text{Leq}}\right)^2 + X_S^2} + j\left(X_P - \frac{\omega^2 M^2 X_S}{\left(R_S + R_{\text{Leq}}\right)^2 + X_S^2}\right). \tag{14}$$

The input impedance angle θ_P is given by

$$\theta_P = \arctan\left(\frac{\text{Im}\left(Z_{\text{IN}}\right)}{\text{Re}\left(Z_{\text{IN}}\right)}\right) \tag{15}$$

where $\text{Re}(Z_{\text{IN}})$ and $\text{Im}(Z_{\text{IN}})$ represent the real and imaginary parts of Z_{IN}, respectively.

Fig. 4 shows the variation of θ_P against M and α, subject to constraint given in (13). As can be observed, the surface of θ_P that intersects with ZPA plane is a single line, and this line indicates the optimal α that satisfies the ZPA condition for any given M.

The equivalent load resistor R_{LeqO} that satisfies the rated power condition is given by (12), whereas R_{LeqZ} that satisfies the ZPA condition when $\text{Im}(Z_{\text{IN}}) = 0$ is given by

$$R_{\text{LeqZ}}\left|\text{Im}\left(Z_{\text{IN}}\right) = 0 = \sqrt{\frac{X_S}{X_P}} \cdot \sqrt{\omega^2 M^2 - X_P X_S} - R_S. \tag{16}$$

Accordingly and as shown by the intersection line in Fig. 4, α satisfies both conditions only when

$$R_{\text{LeqO}}\left(\alpha\right) = R_{\text{LeqZ}}. \tag{17}$$

Therefore, the optimal value α_{opt} that corresponds to ZPA can be determined first by solving (17), and then the optimal value of β for constant power can be found from (13) using the optimal α. In summary, the combinations of α and β, determined from (13) and (17), are the optimal duty cycles of converters that correspond to maintaining constant output power at the ZPA condition despite any variations in inductances due to pad misalignment.

$$R_{\text{LeqO}} = \frac{Z_{\text{M}}^2 V_{\text{P}}^2 - 2K_1 P_{\text{out}} - \sqrt{Z_{\text{M}}^4 V_{\text{P}}^4 - 4Z_{\text{M}}^2 V_{\text{P}}^2 K_1 P_{\text{out}} - 4K_2^2 P_{\text{out}}^2}}{2P_{\text{out}}\left(X_{\text{P}}^2 + R_{\text{P}}^2\right)} \tag{12}$$

D. ZPA Point as the Optimal Efficiency Point

The system efficiency can be derived by considering the ratio of output to input power as given by

$$\eta = \frac{P_{\text{out}}}{P_{\text{in}}} = \frac{\omega^2 M^2 R_{\text{Leq}}}{\omega^2 M^2 (R_S + R_{\text{Leq}}) + R_P \left[(R_S + R_{\text{Leq}})^2 + X_S^2 \right]}. \tag{18}$$

By setting the derivative of η with respect to R_{Leq} to zero, the optimal-efficiency load resistor $R_{\text{Leq}M}$ can be obtained as

$$R_{\text{Leq}M} = \sqrt{\frac{R_S}{R_P}} \cdot \sqrt{\omega^2 M^2 + R_P R_S + \frac{R_P}{R_S} X_S}. \tag{19}$$

From (16) and (19), it is evident that the two equations are of similar form and have the common term $\omega^2 M^2$. Usually, $\omega^2 M^2$ is much larger than the other terms, and therefore (16) and (19) can be approximated as

$$R_{\text{Leq}Z} \approx \sqrt{\frac{X_S}{X_P}} \cdot \sqrt{\omega^2 M^2} = \sqrt{r_X}\omega M \tag{20}$$

$$R_{\text{Leq}M} \approx \sqrt{\frac{R_S}{R_P}} \cdot \sqrt{\omega^2 M^2} = \sqrt{r_{Xm}}\omega M. \tag{21}$$

If the ratio $r_X = X_S / X_P$ is designed to be approximately equal to the ratio $r_{Xm} = R_S / R_P$, then the following relationship can be established:

$$R_{\text{Leq}M} \approx R_{\text{Leq}Z} = R_{\text{Leq}O}(\alpha_{\text{opt}}). \tag{22}$$

This is because if the ratio between primary and secondary coil turns is N ($N \geq 1$), then the inductance ratio of the two coils is proportional to or less than N^2, and the resistance ratio of the two coils is proportional to N. Accordingly, $r_X \geq 1/N^2$ whereas $r_{Xm} = 1/N$. Thus, the ratio between $R_{\text{Leq}M}$ and $R_{\text{Leq}Z}$ is less than $\sqrt{N}$. Usually, N is in the range of 1–1.5, therefore the difference between $R_{\text{Leq}M}$ and $R_{\text{Leq}Z}$ is relatively small.

Equation (22) satisfies the condition for constant output power operation of the system with the ZPA at optimal efficiency. Moreover, it is easier to satisfy (22) with symmetric charging coils having the same self-inductances and ESRs, and then ZPA operation ensures optimal efficiency. For asymmetric charging coils, whether (22) can be satisfied depends on the variation of self-inductance and how compensation capacitors are designed and this aspect needs detailed analysis in such situations.

Fig. 5 shows the variation of system efficiency against M for various α. For each fixed α, the system efficiency reaches the maximum for only one value of M but decreases with other values of M. However, it should be noted that the system efficiency η is maximum irrespective of the value of M when α equals α_{opt} given in (17).

The rms values of primary and secondary resonant currents are shown in Fig. 6. The variations of currents are in accordance with the system efficiency. For symmetrical coils, it is expected to have balanced primary and secondary currents. When $\alpha = 60°$, I_P and I_S intersects at $M = 15\ \mu$H. However, when M increases, the difference between I_P and I_S becomes large, resulting in larger losses in coils. When α equals α_{opt}, I_P and I_S are not the minimum currents, but remain equal in magnitude, to minimize total coil losses.

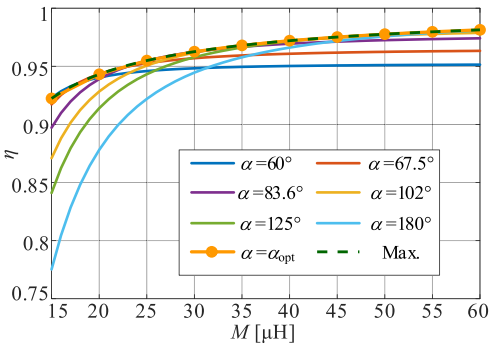

Fig. 5. System efficiency with various α versus M.

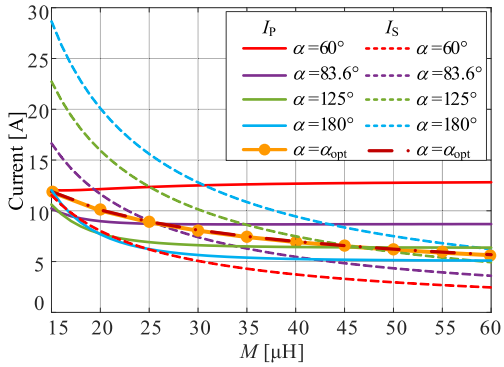

Fig. 6. Primary and secondary currents with various α versus M.

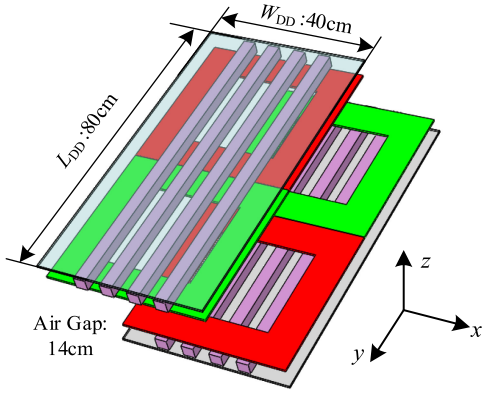

Fig. 7. Structure of the DD pads.

III. Parameter Analysis

A. Influence of Self-Inductance

In Section II, X_P and X_S were assumed to be constant for simplification. In fact, the self-inductances of coils with ferrite cores vary with misalignment due to change in magnetic reluctance with the displacement. In this article, DD type pads are used as the charging coils, and x represents the misalignment along X-direction, as shown in Fig. 7. Variations of measured mutual M, self-inductances L_P and L_S with misalignment are shown in Fig. 8 and, as evident, all inductances decrease with increasing x.

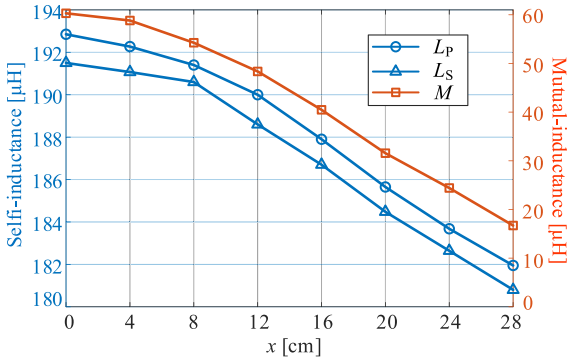

Fig. 8. Variation in self- and mutual inductances with coil misalignment.

The maximum variation of L_P (L_S) is about 10.9 μH (10.7 μH) corresponding to the variation in reactance by 5.82 Ω (5.71 Ω).

In order to demonstrate how the variation in L_P and L_S affects the currents, the nominalized self-inductances L_P/L_{Pm} (L_S/L_{Sm}) within the range from 100% to 95% are considered, while maintaining the mutual inductance at 20 μH. With each L_P and L_S, α and β were solved according to (17) and (13) to satisfy rated output power and ZPA condition, using the voltage parameters in Table I. Then the primary current I_P and the secondary current I_S can be solved.

Fig. 9(a) shows the primary current I_P versus L_P/L_{Pm} and L_S/L_{Sm}. It is evident that I_P increases with smaller L_S but decreases with smaller L_P. In contrast, the variation in L_P and L_S has an opposite effect on I_S, as can be seen from Fig. 9(b). Therefore, simultaneous minimization of both I_P and I_S is quite difficult to achieve, as minimum I_P corresponds to the maximum I_S, and vice versa. A better approach is to balance currents on both sides to reduce the losses.

The system efficiency η as a function of X_P and r_X is plotted in Fig. 10. X_P was set to 0.5, 2.5, and 3 Ω to investigate the sensitivity of the system efficiency to the absolute value of reactance. Moreover, r_X was varied from 0.2 to 5 to show how the difference between X_P and X_S affects the system efficiency. For each X_P and X_S, α and β were solved according to (17) and (13) while satisfying the rated output power and ZPA condition. Then η was calculated through (6) and (18).

First, it can be noted that the maximum point of each curve corresponds to $r_X = 1$. That is, under specified condition, the system efficiency reaches the maximum when $X_P = X_S$ as evident from (20) and (21). Second, the larger the mutual inductance, the higher is the system efficiency, as expected. Third, the system η is more sensitive to r_X when M is small, and for large values of M, the variation of X_P and X_S has minor effect on η. Therefore, if r_X is designed to be equal to r_{Xm}, then operation at optimal efficiency can be achieved despite coil misalignments.

B. Design of Cp and Cs

C_P and C_S should be selected properly, keeping r_X as close as possible to the ratio r_{Xm}. Therefore, it is preferable to use symmetrical primary and secondary coils. This is because R_P and R_S are almost the same ($r_{Xm} = 1$) and the variations

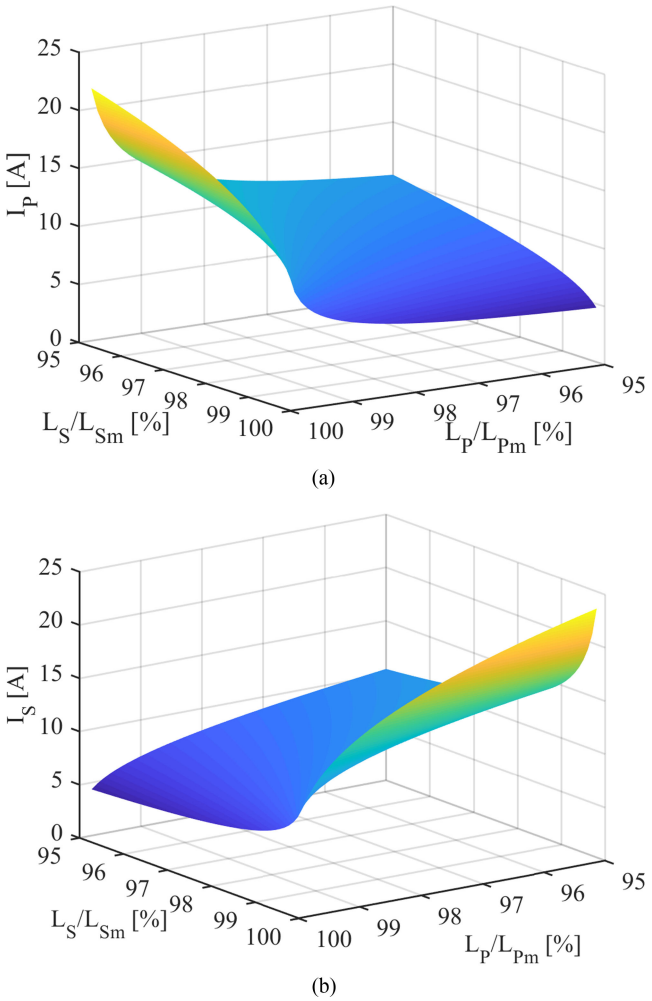

Fig. 9. Influence of X_P and X_S on currents. (a) Primary current I_P versus X_P and X_S. (b) Secondary current I_S versus X_P and X_S.

in L_P and L_S are also similar, which makes the selection of C_P and C_S simpler. In this article, symmetrical DD pads were used, and the measured self- and mutual inductances of which are shown in Fig. 8. There are two ways to select C_P and C_S. In the first approach $1/\omega C_P$ ($1/\omega C_S$) is set to be larger than $\omega L_{P\max}$ ($\omega L_{S\max}$) where $L_{P\max}$ ($L_{S\max}$) is the largest self-inductance of the primary (secondary) coil as, in this case, X_P (X_S) is always negative and the capacitive reactance increases with misalignment. In the second approach, $1/\omega C_P$ ($1/\omega C_S$) is set to be smaller than $\omega L_{P\min}$ ($\omega L_{S\min}$) where $L_{P\min}$ ($L_{S\min}$) is the minimum self-inductance at the largest misalignment. The largest misalignment is dictated by output power level and the maximum primary current as, in this case, X_P (X_S) is always positive, and the inductive reactance reaches the maximum when the coils are in alignment. Because the system efficiency is more sensitive to reactance when M is small, C_P and C_S should be selected to reduce X_P and X_S during large misalignments. Thus, the second approach is preferred.

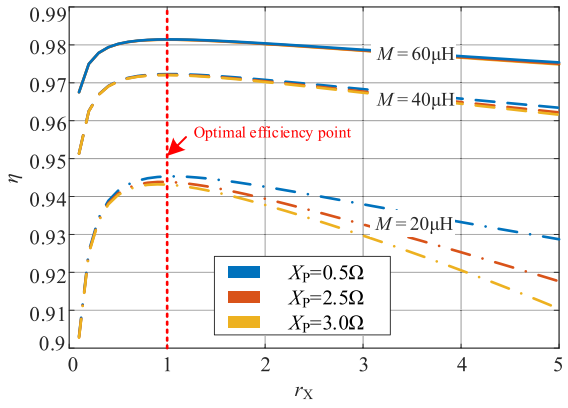

Fig. 10. System efficiency with various ratio of X_P and X_S.

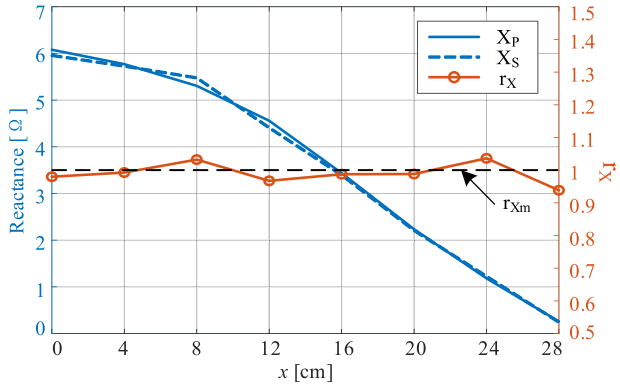

Fig. 11. X_P and X_S versus misalignment position x.

In this article, the position $x = 28$ cm where M is 16.7 μH and the coupling factor k is 0.09 is chosen as the largest misalignment. The minimum self-inductances $L_{P\min}$ and $L_{S\min}$ equal to 181.95 and 180.8 μH at this misalignment, and $\Delta L = 0.5$ μH was considered for the initial value of X_P and X_S. So, C_P and C_S can be calculated as

$$C_P = \frac{1}{\omega^2 (L_{P\min} - \Delta L)} = 19.32 \text{ nF} \tag{23}$$

$$C_S = \frac{1}{\omega^2 (L_{S\min} - \Delta L)} = 19.44 \text{ nF}. \tag{24}$$

Fig. 11 shows the variation of X_P and X_S against misalignment with C_P (19.32 nF), C_S (19.44 nF), and the self-inductance data in Fig. 7. The maximum X_P and X_S are 6.08 and 5.96 Ω, respectively, and occur at the position $x = 0$ cm. The minimum X_P and X_S are 0.26 and 0.24 Ω, and occur at position $x = 28$ cm. The actual ratio r_X of X_S and X_P is close to r_{Xm}, and the error between r_X and r_{Xm} is less than 10%. According to Fig. 10, the efficiency drop caused by the error in r_X is less than 0.1%. Therefore, the error in r_X, which may be caused by the variations in C_P (C_S) and L_P (L_S), can be ignored. In addition, even though the maximum X_P is 6.08 Ω, the system efficiency can still be high because M is large and the system efficiency is not sensitive to X_P (X_S).

C. Design of DC Voltage

For S–S compensation network, the output power is inversely proportional to M, and the power transfer capability is limited by the maximum mutual inductance $M_{\max}$. In order to guarantee the delivery of rated output power under optimal load condition over the entire misalignment range, the dc voltages $V_{\rm dc}$ and $V_{\rm o}$, $M_{\max}$, and the rated power $P_{\rm out,rated}$ must be carefully matched. Moreover, $\alpha = \beta = \pi$ should correspond to the maximum input voltage V_P and the maximum equivalent load resistor $R_{\rm Leq}$ respectively. If $\alpha = \beta = \pi$ can satisfy the required power and optimal load condition under $M_{\max}$, then the optimal combinations of α and β under varying (smaller) mutual inductances can always be found.

For the secondary converter with $\beta = \pi$, the maximum $R_{\rm Leq}$ for rated power can be expressed by

$$R_{\rm Leq,max} = \frac{8}{\pi^2}\sin\left(\frac{\pi}{2}\right)^2 R_L = \frac{8}{\pi^2}\frac{V_O^2}{P_{\rm out,rated}}. \tag{25}$$

In order to satisfy the ZPA condition in (20) and the optimal efficiency condition in (21), $R_{\rm Leq,max}$ should be equal or larger than

$$R_{\rm Leq,max} = \frac{8}{\pi^2}\frac{V_O^2}{P_{\rm out,rated}} \geq \omega M_{\max}. \tag{26}$$

Substituting (26) and (5) with $\alpha = \pi$ into (12), the rated output power with optimal efficiency condition can be derived as an implicit function of $V_{\rm dc}$ as expressed by (27) shown at the bottom of the next page. Equations (26) and (27) are the conditions that $V_{\rm dc}$, V_o, $M_{\max}$, and $P_{\rm out,rated}$ should match to ensure the delivery of rated power at optimal efficiency over the entire misalignment range.

For example, $M_{\max}$ is 60.3 μH and $P_{\rm out,rated}$ is set as 1 kW in this article. The dc voltages $V_{\rm dc}$ and V_o are the variables to be designed. R_P (R_S) is set to 0.3 Ω (0.3 Ω) and L_P (L_S) is set as same as the self-inductance in Fig. 8 at $x = 0$ cm. The dc voltage $V_{\rm dc}$ satisfying (27) can be calculated as 197.5 V and is rounded up to 200 V. According to (26), the dc voltage V_O can be calculated as 198.8 V and is rounded up to 200 V. As a result, the equivalent dc resistor R_L is 40 Ω, and $R_{\rm Leq,max}$ is 32.4 Ω, which matches $\omega M_{\max} = 32.2$ Ω. Therefore, both $V_{\rm dc}$ and V_o are designed as 200 V in this article for theoretical analysis and experimental verifications.

Generally, (26) and (27) are the necessary conditions that ensure the proposed control method is effective over the entire misalignment range. In practice, the mutual inductance $M_{\max}$ can also be designed to satisfy power requirement with a constrained voltage rating, or alternatively the maximum power rating can be evaluated for a given $M_{\max}$ and dc voltages.

IV. Control Strategy

According to the analysis presented in Section II, the two control goals in the proposed method are to (1) maintain rated output power through regulation of output current (2) operate the primary-side converter with ZPA. The proposed control strategy allows both converters to operate independently with control freedom to achieve these two goals. Moreover, there is no

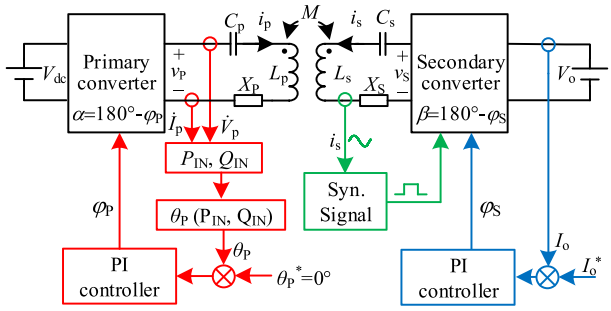

Fig. 12. Control block diagram of the proposed method.

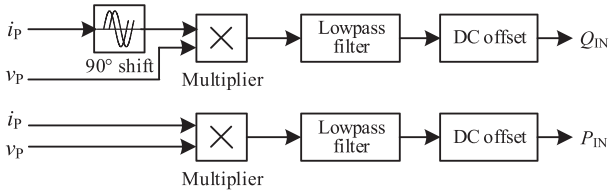

Fig. 13. Block diagram of *PQ* processing circuit [26].

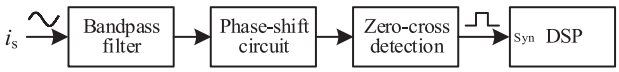

Fig. 14. Block diagram of the synchronization signal circuit.

necessity for wireless communication between the primary and the secondary, as the secondary converter, serving as a controlled rectifier, controls the output current while the primary converter, serving as an inverter, controls the input voltage V_P with ZPA.

The block diagram of the proposed control philosophy is illustrated in Fig. 12. On the primary side, the input voltage v_P and the primary current i_P are sampled to calculate the input active power $P_{\rm IN}$ and the reactive power $Q_{\rm IN}$ with a signal processing circuit used in [26], as shown in Fig. 13. The product of i_P and v_P generates the real-time active power signal. The current i_P is shifted with 90° and then is multiplied by v_P to generate the real-time reactive power signal. The two signals are filtered by low-pass filters and are offset to be positive dc signals that are proportional to $P_{\rm IN}$ and $Q_{\rm IN}$ respectively. They can be sampled by the analog–digital module in a digital signal processor (DSP). When $P_{\rm IN}$ and $Q_{\rm IN}$ are known, the input impedance angle θ_P can be solved as

$$\theta_P = \arcsin\left(\frac{Q_{\rm IN}}{\sqrt{P_{\rm IN}^2+Q_{\rm IN}^2}}\right). \tag{28}$$

A PI controller generates φ_P of the primary converter to control θ_P to be zero.

In the secondary side, the output current I_O is measured and compared by the reference value I_O^*. A PI controller generates φ_S of the secondary converter according to the output current

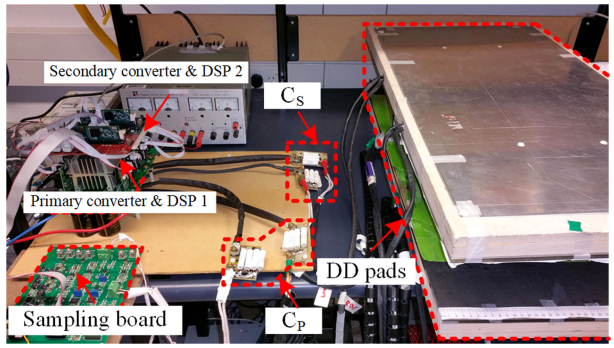

Fig. 15. Experimental prototype.

error. Because the equivalent load is resistive, the input voltage v_S of the secondary converter should be in phase with the secondary current i_S. Thus, the PWM driving signals of the secondary converter are synchronized with i_S by a synchronization signal circuit as shown in Fig. 14. Through a bandpass filter, a phase-shift circuit and a zero-cross detection circuit, the sinusoidal i_S is converted to a square wave to generate the synchronization signal to the DSP in the secondary side.

Although both the primary and secondary PI controllers work independently, the convergence of the system is guaranteed due to monotonic characteristics of β and θ_P with respect to α. As evident in (13) and Fig. 3, β is a monotonic function of α under given output power. For the secondary converter, β is not changed arbitrarily to regulate the output power but it is inversely proportional to α and should comply with the output power constraint. If α is increased, β has to be decreased to regulate output power. Meanwhile, according to (6) and (15), the variation of β leads to the change of $R_{\rm Leq}$ and θ_P. Consequently, θ_P is also a monotonic function of α as shown in Fig. 4. If the measured θ_P is larger than zero, α is increased and β is decreased, leading to the decrease of θ_P. If the measured θ_P is smaller than zero, α is decreased and β is increased, resulting in the increase of θ_P. Consequently and with time, α gradually approaches the optimal value that is required for ZPA, whereas β reaches the optimal value that is required for rated power. Accordingly, a closed-loop controller with the parameters designed in Section III guarantees that optimal α and β can always be achieved.

V. Experimental Validation

A 1-kW experiment prototype, as shown in Fig. 15, was designed, built, and operated to validate the proposed concept. Two DD pads are separated by 14-cm air-gap and their physical size is shown in Fig. 7. The pad misalignment range is [0, 20] cm, corresponding to the mutual inductance range between 60.3 and 31.6 μH. The circuit parameters of the prototype are listed in Table II, and the PI controllers, used for regulating the output

$$\omega M_{\max} = \frac{\frac{4}{\pi^2}Z_M^2V_{\rm dc}^2 - K_1P_{\rm out,rated} - \sqrt{\frac{16}{\pi^2}Z_M^4V_{\rm dc}^4 - \frac{8}{\pi^2}Z_M^2V_{\rm dc}^2K_1P_{\rm out,rated} - K_2^2P_{\rm out,rated}^2}}{P_{\rm out,rated}\left(X_P^2+R_P^2\right)} \tag{27}$$

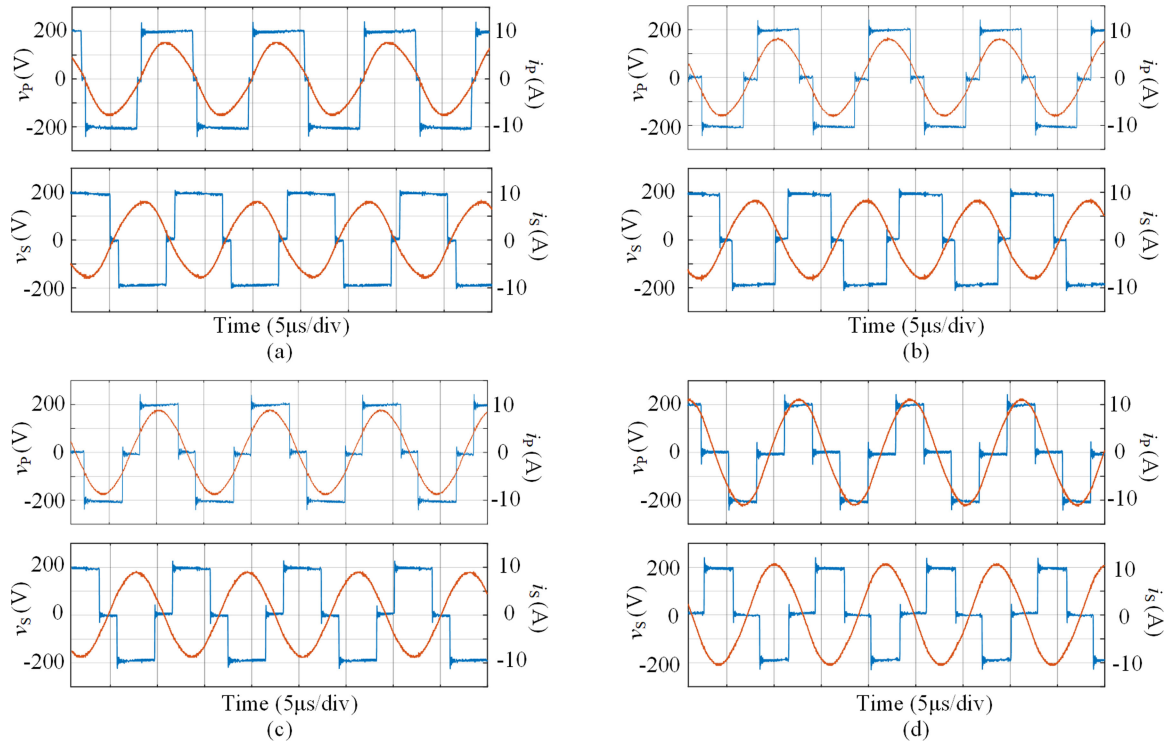

Fig. 16. Steady-state waveforms of the primary and secondary converters. (a) $x = 0$ cm. (b) $x = 8$ cm. (c) $x = 12$ cm. (d) $x = 20$ c.

TABLE II
PARAMETERS OF THE EXPERIMENT PROTOTYPE

Symbol	Parameter	Value	Unit
f	inverter frequency	85	kHz
V_{dc}	input voltage	200	V
V_{out}	output voltage	200	V
L_P	inductance of primary coil	[192.9, 185.6]	μH
C_P	compensation capacitor of L_P	18.9	nF
R_P	ESR of primary coil	0.3	Ω
L_S	inductance of secondary coil	[191.5, 184.5]	μH
C_S	compensation capacitor of L_S	19	nF
R_S	ESR of secondary coil	0.3	Ω
M	mutual inductance	[60.3, 31.6]	μH

current and the ZPA condition, were implemented in two DSPs (TMS320F28335) located on the primary and secondary sides. All waveforms were recorded using an Agilent DSO-X 3034A oscilloscope.

The steady-state waveforms of primary output voltage v_P, primary current i_P, secondary voltage v_S, and secondary current i_S at four misaligned positions are shown in Fig. 16. When coils were aligned at $x = 0$ cm, α and β are close to 180°, the voltage waveforms are shifted by 90^0, with primary voltage leading to indicate forward power flow. With more misalignment indicated by increasing x, the secondary-side duty cycle β is decreased to regulate the output current, whereas primary-side duty cycle α is also decreased to control to maintain θ_P at zero. It is observable that currents i_P and i_S are balanced at each misaligned position, and increase with larger misalignment.

In order to show the feasibility and effectiveness of the proposed control method, the prototype system was tested using a closed-loop controller. Fig. 17 shows the primary current i_P, secondary current i_S, output current I_O, and the measured $Q_{\rm IN}$ when the system was operated detuned at position $x = 0$ cm, where X_P and X_S reach maximum. During the interval between 0s and 2.3s, the system was operated in open loop, and α and β were set to be 180° and 90° respectively. The output current I_O was only 2.6 A (corresponding to 520 W output power) and the measured $Q_{\rm IN}$ was 150 Var, which were far from the reference values (5 A/1000 W, 0 Var). The controller was introduced at 2.3 s. Then the output current I_O was regulated to be the reference value (5 A, corresponding to 1kW output power), and the measured $Q_{\rm IN}$ signal decreased to zero. The response of the controller when changing the output reference is shown in Fig. 18. During the interval between 0 and 2.4 s, the system was operated with closed-loop control at rated 5-A output current and 1-kW output power, whereas $Q_{\rm IN}$ was regulated at zero. The reference value of I_O was changed from 5–3 A at 2.4 s, and the actual output current followed the change whereas $Q_{\rm IN}$ was regulated to zero again after a transient increase.

The output power and system efficiency with coil misalignment are shown in Fig. 19. The output power was regulated at 1-kW with coil misalignment, and it can be seen that it was maintained at rated level despite the large coil

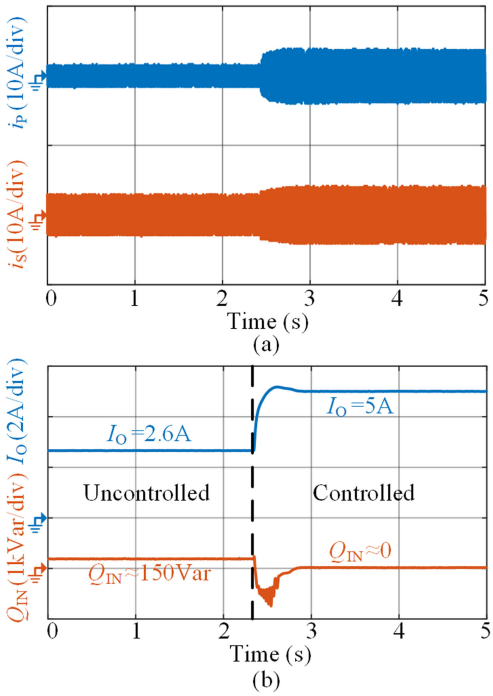

Fig. 17. Transient response when the controller started to work. (a) Waveforms of i_P and i_S. (b) Waveforms of I_O and $Q_{\rm IN}$ signal.

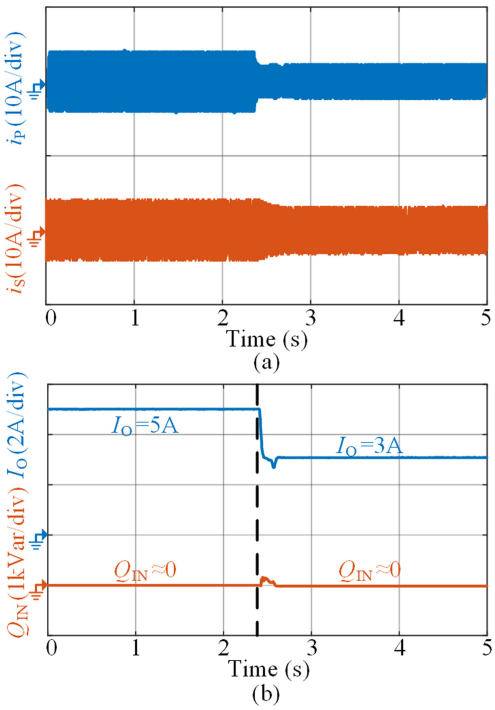

Fig. 18. Transient response when the output reference was changed. (a) Waveforms of i_P and i_S. (b) Waveforms of I_O and $Q_{\rm IN}$ signal.

misalignment. As expected, the maximum efficiency reaches 95.7% when the coils were in alignment but drops to 91.5% at maximum misalignment, which is acceptable for the large misalignment.

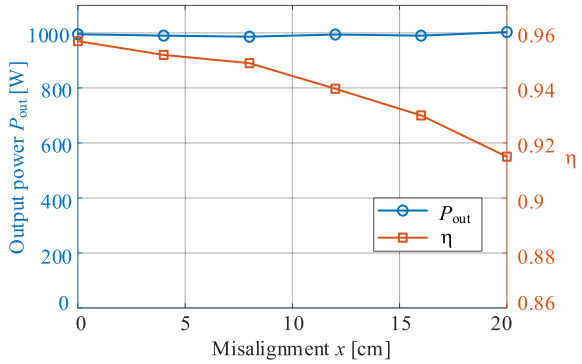

Fig. 19. Measured output power and efficiency with coil misalignment.

VI. Conclusion

A novel control technique that wirelessly charges EVs at rated power level with optimum efficiency, despite large coil misalignments, has been presented. The proposed controller uses the phase angle of input impedance to operate the charger essentially at ZPA and optimal load condition to ensure that charging takes place at rated power with optimal efficiency despite any variations in system parameters due to misalignment. A comprehensive mathematical model, which describes the theoretical basis of the proposed control philosophy, has also been presented. The validity of the proposed control concept has convincingly been demonstrated, presenting measured results of a 1-kW bidirectional WPT EV charging system in comparison to both theoretical results, under misaligned coil conditions. In order to mitigate the adverse effects of hard switching, soft-switched operation of converters could be considered in future research.

Acknowledgment

The authors thank Dr. L. Zhao and Dr. Y. Tang for their help on building the experimental prototype. This work was carried out at the University of Auckland.

References

[1] G. A. Covic and J. T. Boys, "Modern trends in inductive power transfer for transportation applications," *IEEE J. Emerg. Sel. Topics Power Electron.*, vol. 1, no. 1, pp. 28–41, Mar. 2013.
[2] J. M. Miller, P. T. Jones, J. Li, and O. C. Onar, "ORNL experience and challenges facing dynamic wireless power charging of EV's," *IEEE Circuits Syst. Mag.*, vol. 15, no. 2, pp. 40–53, May 2015.
[3] C. C. Mi, G. Buja, S. Y. Choi, and C. T. Rim, "Modern advances in wireless power transfer systems for roadway powered electric vehicles," *IEEE Trans. Ind. Electron.*, vol. 63, no. 10, pp. 6533–6545, Oct. 2016.
[4] U. K. Madawala and D. J. Thrimawithana, "A bidirectional inductive power interface for electric vehicles in V2G systems," *IEEE Trans. Ind. Electron.*, vol. 58, no. 10, pp. 4789–4796, Oct. 2011.
[5] G. Buja, M. Bertoluzzo, and K. N. Mude, "Design and experimentation of WPT charger for electric city car," *IEEE Trans. Ind. Electron.*, vol. 62, no. 12, pp. 7436–7447, Dec. 2015.
[6] R. Bosshard and J. W. Kolar, "Multi-objective optimization of 50 kW/85 kHz IPT system for public transport," *IEEE J. Emerg. Sel. Topics Power Electron.*, vol. 4, no. 4, pp. 1370–1382, Dec. 2016.
[7] S. Y. Choi, B. W. Gu, S. Y. Jeong, and C. T. Rim, "Advances in wireless power transfer systems for roadway-powered electric vehicles," *IEEE J. Emerg. Sel. Topics Power Electron.*, vol. 3, no. 1, pp. 18–36, Mar. 2015.

[8] D. Patil, M. K. McDonough, J. M. Miller, B. Fahimi, and P. T. Balsara, "Wireless power transfer for vehicular applications: Overview and challenges," *IEEE Trans. Transp. Electrific.*, vol. 4, no. 1, pp. 3–37, Mar. 2018.
[9] M. Budhia, J. T. Boys, G. A. Covic, and C. Huang, "Development of a single-sided flux magnetic coupler for electric vehicle IPT charging systems," *IEEE Trans. Ind. Electron.*, vol. 60, no. 1, pp. 318–328, Jan. 2013.
[10] A. Zaheer, H. Hao, G. A. Covic, and D. Kacprzak, "Investigation of multiple decoupled coil primary pad topologies in lumped IPT systems for interoperable electric vehicle charging," *IEEE Trans. Power Electron.*, vol. 30, no. 4, pp. 1937–1955, Apr. 2015.
[11] F. Lu, H. Zhang, H. Hofmann, W. Su, and C. C. Mi, "A dual-coupled LCC-compensated IPT system with a compact magnetic coupler," *IEEE Trans. Power Electron.*, vol. 33, no. 7, pp. 6391–6402, Jul. 2018.
[12] L. Zhao, D. J. Thrimawithana, and U. K. Madawala, "Hybrid bidirectional wireless EV charging system tolerant to pad misalignment," *IEEE Trans. Ind. Electron.*, vol. 64, no. 9, pp. 7079–7086, Sep. 2017.
[13] L. Zhao, D. J. Thrimawithana, U. K. Madawala, A. P. Hu, and C. C. Mi, "A misalignment-tolerant series-hybrid wireless EV charging system with integrated magnetics," *IEEE Trans. Power Electron.*, vol. 34, no. 2, pp. 1276–1285, Feb. 2019.
[14] J. M. Miller, O. C. Onar, and M. Chinthavali, "Primary-side power flow control of wireless power transfer for electric vehicle charging," *IEEE J. Emerg. Sel. Topics Power Electron.*, vol. 3, no. 1, pp. 147–162, Mar. 2015.
[15] K. Colak, E. Asa, M. Bojarski, D. Czarkowski, and O. C. Onar, "A novel phase-shift control of semibridgeless active rectifier for wireless power transfer," *IEEE Trans. Power Electron.*, vol. 30, no. 11, pp. 6288–6297, Nov. 2015.
[16] D. J. Thrimawithana, U. K. Madawala, and M. Neath, "A synchronization technique for bidirectional IPT systems," *IEEE Trans. Ind. Electron.*, vol. 60, no. 1, pp. 301–309, Jan. 2013.
[17] M. J. Neath, A. K. Swain, U. K. Madawala, and D. J. Thrimawithana, "An optimal PID controller for a bidirectional inductive power transfer system using multiobjective genetic algorithm," *IEEE Trans. Power Electron.*, vol. 29, no. 3, pp. 1523–1531, Mar. 2014.
[18] T. Diekhans and R. W. De Doncker, "A dual-side controlled inductive power transfer system optimized for large coupling factor variations and partial load," *IEEE Trans. Power Electron.*, vol. 30, no. 11, pp. 6320–6328, Nov. 2015.
[19] B. X. Nguyen *et al.*, "An efficiency optimization scheme for bidirectional inductive power transfer systems," *IEEE Trans. Power Electron.*, vol. 30, no. 11, pp. 6310–6319, Nov. 2015.
[20] R. Mai, Y. Liu, Y. Li, P. Yue, G. Cao, and Z. He, "An active-rectifier-based maximum efficiency tracking method using an additional measurement coil for wireless power transfer," *IEEE Trans. Power Electron.*, vol. 33, no. 1, pp. 716–728, Jan. 2018.
[21] M. Fu, H. Yin, X. Zhu, and C. Ma, "Analysis and tracking of optimal load in wireless power transfer systems," *IEEE Trans. Power Electron.*, vol. 30, no. 7, pp. 3952–3963, Jul. 2015.
[22] T. Yeo, D. Kwon, S. Khang, and J. Yu, "Design of maximum efficiency tracking control scheme for closed-loop wireless power charging system employing series resonant tank," *IEEE Trans. Power Electron.*, vol. 32, no. 1, pp. 471–478, Jan. 2017.
[23] W. X. Zhong and S. Y. R. Hui, "Maximum energy efficiency tracking for wireless power transfer systems," *IEEE Trans. Power Electron.*, vol. 30, no. 7, pp. 4025–4034, Jul. 2015.
[24] X. Dai, X. Li, Y. Li, and A. P. Hu, "Maximum efficiency tracking for wireless power transfer systems with dynamic coupling coefficient estimation," *IEEE Trans. Power Electron.*, vol. 33, no. 6, pp. 5005–5015, Jun. 2018.
[25] W. Zhong and S. Y. R. Hui, "Charging time control of wireless power transfer systems without using mutual coupling information and wireless communication system," *IEEE Trans. Ind. Electron.*, vol. 64, no. 1, pp. 228–235, Jan. 2017.
[26] Y. Tang, Y. Chen, U. K. Madawala, D. J. Thrimawithana, and H. Ma, "A new controller for bidirectional wireless power transfer systems," *IEEE Trans. Power Electron.*, vol. 33, no. 10, pp. 9076–9087, Oct. 2018.

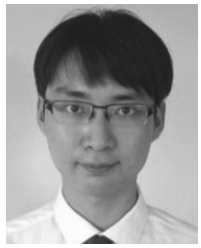

Yeran Liu (S'17) received B.Sc. degree in electrical engineering from the School of Electrical Engineering, Southwest Jiaotong University, Emei, China, in 2015. He is currently working toward the Ph.D. degree in electrical engineering in the School of Electrical Engineering, Southwest Jiaotong University, Chengdu, China.

His current research includes wireless power transfer.

Udaya Kumara Madawala (S'88–M'93–SM'06–F'18) received the B.Sc. (Hons.) degree in electrical engineering from the University of Moratuwa, Moratuwa, Sri Lanka, in 1986, and the Ph.D. degree in power electronics from The University of Auckland, Auckland, New Zealand, in 1993, as a Commonwealth Doctoral Scholar.

He is currently a Full Professor. He has more than 250 IEEE and IET journal and international conference publications and holds a number of patents related to wireless power transfer and power converters. His research interests include power electronics, wireless power transfer, vehicle-to-grid applications, and renewable energy.

Dr. Madawala is a Distinguished Lecturer of the IEEE Power Electronic Society, and has more than 30 years of both industry and research experience in the fields of power electronics and energy. He has served both the IEEE Power Electronics and Industrial Electronics Societies in numerous roles, relating to conferences, technical committees, and chapter activities. He is currently an Associate Editor for the IEEE TRANSACTIONS ON POWER ELECTRONICS, and a Member of the Sustainable Energy Systems Technical Committee and the Oceania Liaison Chair of Membership Development Committee of the IEEE Power Electronics Society.

Ruikun Mai (M'14) received B.Sc. and Ph.D. degree in electrical engineering from the School of Electrical Engineering from Southwest Jiaotong University, Chengdu, China, 2004 and 2010, respectively.

He is currently a Professor with the School of Electrical Engineering, Southwest Jiaotong University. His research interests include wireless power transfer and its application in railway systems, power system stability, and control.

Zhengyou He (M'10–SM'13) received the B.Sc. and M. Sc. degrees in computational mechanics from Chongqing University, Chongqing, China, in 1992 and 1995, respectively, and the Ph.D. degree in electrical engineering from the School of Electrical Engineering, Southwest Jiaotong University, Chengdu, China, in 2001.

He is currently a Professor with the School of Electrical Engineering, Southwest Jiaotong University. His research interests include signal process and information theory applied to the electrical power system, and the application of wavelet transforms in power system.